PNAS RESEARCH ARTICLE | PHYSICS

The Role of Spin-Flip Collisions in a Dark-Exciton Condensate

Subhradeep Misra[a], Michael Stern[b], Vladimir Umansky[a], and Israel Bar-Joseph[a,1]

Edited by David Snoke, University of Pittsburgh, Pittsburgh, PA; received February 27, 2022; accepted June 1, 2022 by Editorial Board Member Shaul Mukamel

We show that a Bose–Einstein condensate consisting of dark excitons forms in GaAs coupled quantum wells at low temperatures. We find that the condensate extends over hundreds of micrometers, well beyond the optical excitation region, and is limited only by the boundaries of the mesa. We show that the condensate density is determined by spin-flipping collisions among the excitons, which convert dark excitons into bright ones. The suppression of this process at low temperature yields a density buildup, manifested as a temperature-dependent blueshift of the exciton emission line. Measurements under an in-plane magnetic field allow us to preferentially modify the bright exciton density and determine their role in the system dynamics. We find that their interaction with the condensate leads to its depletion. We present a simple rate-equations model, which well reproduces the observed temperature, power, and magnetic-field dependence of the exciton density.

excitons | Bose–Einstein condensation | quantum wells | GaAs | optical spectroscopy

Significance

Bound electron-hole pairs in semiconductors, known as excitons, can recombine through light emission (labeled "bright") or through nonradiative processes (labeled "dark"), depending on the spin orientation of the constituent particles. At low temperatures, they are predicted to undergo Bose–Einstein condensation, with the dark excitons occupying the ground state. In this work, we study photo-excited excitons in GaAs/AlGaAs coupled quantum wells. We show that a high-density condensate of dark excitons forms at cryogenic temperatures and spreads over a few hundred micrometers, well beyond the excitation region. We find that spin-flip collisions among the excitons, which convert dark excitons to bright, play a dominant role in determining the condensate dynamics and steady-state density.

In the dilute limit, excitons can be considered as a Bose gas and are thus expected to undergo a Bose–Einstein condensation (BEC) transition at low temperatures (1, 2). Over the past few decades, there have been many attempts to realize such a condensate in various material systems. A particularly interesting research direction, which attracted considerable attention, is using indirect excitons (IXs) in coupled quantum well (CQW) structures (3–6). An attractive feature of this system is its long lifetime, which allows achievement of the critical condensation density at moderate excitation powers and establishing quasi-equilibrium at low temperatures. Indeed, a bulk of experimental works on CQW reported a behavior that is consistent with an exciton BEC transition at low temperatures (7–17).

An important development in the quest for the exciton BEC was introduced a little over a decade ago by Combescot et al. (18, 19), who argued that the condensate should be dark. Their argument was based on the fact that electron-hole exchange interaction removes the degeneracy between the bright ($J_z = \pm 1$) and dark ($J_z = \pm 2$) exciton energies, where J_z is z-plane projection of the total angular momentum, such that the dark exciton is lower in energy than the bright one, and hence, it should be the ground state for condensation. Indeed, a series of studies performed in the past decade provided evidence for the formation of a dark condensate (9, 11, 12, 14, 16), with the most compelling one coming from measurement of the IX peak energy increment (blueshift, \Delta E) as the temperature is decreased at constant illumination power (12). ΔE is due to the dipole–dipole repulsive interaction among excitons and is proportional to their density (20). Hence, its increase at low temperatures can be interpreted as a signature of a buildup of long-lived dark excitons at the ground state of the system.

The unique composition of the system, of a thermal part consisting of short-lived bright excitons and a condensate of long-lived dark excitons, poses a challenge in understanding its formation dynamics. It can be viewed as an intermediate case between an atomic BEC, with a fixed number of particles, and a cavity-polaritons condensate, whose steady-state density is set by its fast radiative recombination. Indeed, these conflicting views are manifested in the literature, where some consider it an equilibrium system (5, 6), while others argue that its density is determined by nonradiative recombination processes (21).

In this work, we address this challenge by conducting spectroscopic studies of GaAs/AlGaAs CQW in a mesa structure. We first present conclusive evidence that a dark condensate is formed in this structure at low temperatures and extends over hundreds of micrometers, well beyond the optical excitation region. We then study its formation dynamics and show that its steady-state density is determined by spin-flipping collisions between excitons, which convert dark excitons into bright ones. We show that the inhibition of these processes at low temperatures (T), $T < 3$ K, gives rise to the condensate density buildup.

Evidence for Dark Exciton Condensation

The sample structure is illustrated in Fig. 1. It consists of a CQW system with two GaAs wells having widths of 12 and 18 nm, respectively, separated by an $Al_{0.28}Ga_{0.72}As$

Author affiliations: [a]Department of Condensed Matter Physics, Weizmann Institute of Science, Rehovot 7610001, Israel; and [b]Department of Physics and Center for Quantum Entanglement Science and Technology, Bar-Ilan University, Ramat-Gan 5290002, Israel

Author contributions: S.M. and I.B.J. designed research; S.M. performed research; V.U. grew the high-quality molecular beam epitaxy wafer; S.M. analyzed data; S.M., M.S., and I.B.J. wrote the paper; S.M, M.S., and I.B.J contributed to the interpretation of the results.

The authors declare no competing interest.

This article is a PNAS Direct Submission. D.W.S. is a guest editor invited by the Editorial Board.

[1]To whom correspondence may be addressed. Email: ibj@weizmann.ac.il.

This article contains supporting information online at http://www.pnas.org/lookup/suppl/doi:10.1073/pnas.2203531119/-/DCSupplemental.

Published August 3, 2022.

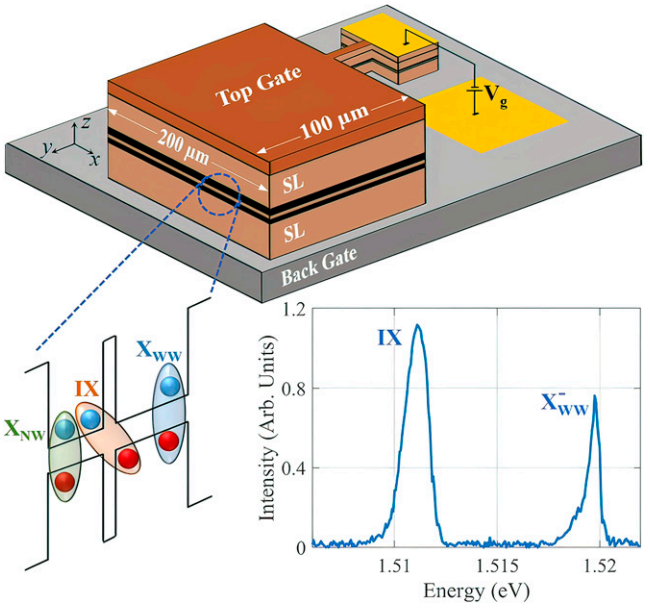

Fig. 1. (*Top*) Schematic diagram of the sample structure. The black stripes at the middle region denote the CQW. (Bottom left) The band diagram of this region under a negative gate voltage, showing the wide-well exciton, X_{WW}, the narrow-well exciton (X_{NW}) and the indirect exciton IX. (Bottom *Right*): An exemplary PL spectrum, taken at $V_g = -3.3$ V, P = 10 μW, and T = 1.7 K. The IXs and the negatively charged wide-well trion (X^-_{WW}) are labeled. (Arb., arbitrary).

barrier of thickness of 3 nm. The CQW is embedded in a 2-μm thick $n^+ - i - n^+$ structure having top and bottom silicon-doped n^+ layers of $Al_{0.12}Ga_{0.88}As$ ($n \sim 10^{18}$ cm^{-3}) that allows application of a voltage perpendicular to the growth direction. The different well width allows us to conduct spectroscopic measurements in each well. The sample was processed using optical lithography, isotropic wet etching, and metal deposition technique to form 200 × 100 μm^2 rectangular mesas. Tunneling of the photoexcited carriers gives rise to charge separation and formation of a dipolar exciton. An exemplary spectrum, depicting the photoluminescence (PL) emission from the sample, is shown in Fig. 1.

We begin by presenting several measurements that provide compelling evidence for the accumulation of dark excitons at low temperatures in our sample. Fig. 2*A* shows the IX peak energy, E_{IX}, as a function of temperature at three gate voltages, V_g, while keeping the pump power fixed at $P = 10$ μW. It is seen that E_{IX} shifts to high energies with decreasing temperatures, reaching $\Delta E = 10 - 20$ meV at $T < 1$ K. These large values of ΔE imply that the steady-state exciton density, n, increases considerably as the temperature is lowered under constant excitation power, approaching 10^{11} cm^{-2} at the lowest temperatures.

To confirm the presence of a high IX density, we measure the absorption spectra of the narrow and wide wells. This is done by tuning the energy of the excitation laser near the direct exciton resonance of each well and measuring the generated photocurrent as a function of laser energy. Fig. 2*B* shows the resulting narrow well spectrum as a function of temperature at −3.3 V. The shift of the direct exciton line to higher energies with decreasing temperatures and the broadening of the lower energy trion line are clear manifestations of the presence of a high density of electrons in this well. Measurements conducted in the wide well are presented in *SI Appendix*, *Nonradiative Processes* and show a similar temperature dependence, confirming that a high hole density builds up in the wide well, too. Solving the self-consistent Schrodinger–Poisson equation, assuming equal charges in the two wells, we could reproduce the shift of the direct exciton and obtain a density of $\sim 5 \times 10^{10}$ cm^{-2} at the lowest temperature, in good agreement with $\Delta E = 10$ meV obtained in Fig. 2*A* for this voltage.

To determine whether this increase of density is due to accumulation of bright or dark excitons, we measure the corresponding change of the radiative rate, γ_r. By conducting measurements at various excitation powers and temperatures, we find that γ_r depends primarily on E_{IX} and becomes faster as E_{IX} increases (Fig. 2*C*), reflecting the increased overlap of the electron and hole wave functions as the external electric field is screened. We can therefore conclude that γ_r increases as the temperature is lowered (and E_{IX} increases) and, hence, the steady-state bright exciton density should decrease with decreasing temperature. Furthermore, if we estimate the steady-state density that can be generated at 10-μW pump power using the measured lifetimes, which vary between 20 and 100 ns over the relevant ΔE range, we obtain $0.4 - 2 \times 10^9$ cm^{-2}, far less than the density required to generate ΔE of 10 to 20 meV. It follows that bright exciton buildup cannot explain the observed blueshift, suggesting that excitons, formed by electrons in the narrow well and holes in the wide well, with a much longer lifetime, accumulate at low temperatures. We confirm that the electrons and holes are bound in an excitonic state by measuring the behavior of the IX line in a perpendicular magnetic field: A clear quadratic diamagnetic shift is observed (*SI Appendix*, Fig. S4).

A conclusive proof for the accumulation of dark excitons is provided by measuring the blueshift away from the excitation beam. Fig. 2*D* shows the normalized ΔE of the IX peak energy as a function of position along a horizontal cross-section of the

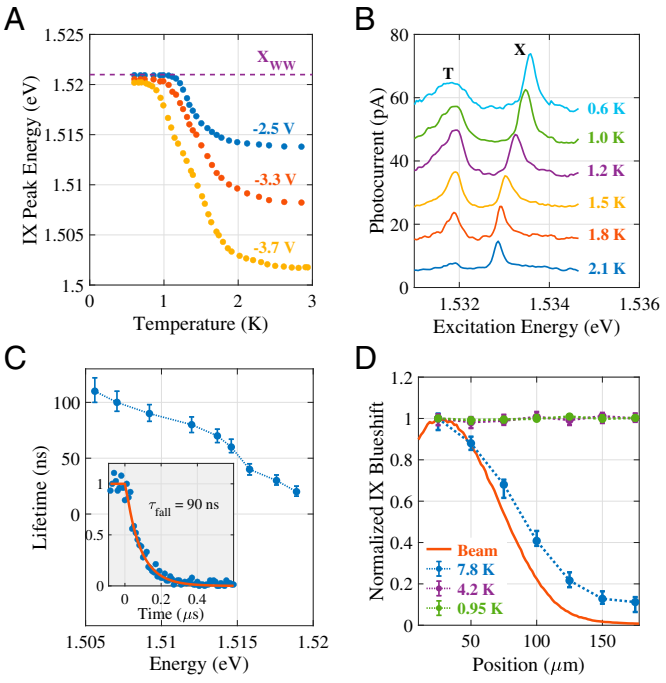

Fig. 2. (*A*) The IX peak energy as a function of temperature at three gate voltages and a fixed power P = 10 μW. The dashed line marks the energy of the wide-well exciton, X_{WW}; (*B*) Photocurrent spectra as the illuminating laser energy is tuned around the narrow-well exciton resonance at various temperatures. Here $V_g = -3.3$ V and P = 2 μW. (*C*) The IX radiative lifetime as a function of peak energy, E_{IX}. (*Inset*) An exemplary trace of the lifetime measurement (blue data points) using correlated photon counting. The red line is a fit to exponential decay, with a fall time of 90 ns. (*D*) The IX blueshift along a horizontal cross-section of the mesa at three temperatures, normalized by its value at the center of the excitation beam (red solid line.) The transition to a constant blueshift at low temperatures can be clearly observed.

mesa, $\Delta E(x)/\Delta E(x=0)$, where $x=0$ is the center of the excitation beam. The measured PL lines as a function of position are given in *SI Appendix*, Fig. S9. Since ΔE is proportional to the exciton density, this measurement yields the density distribution. It is seen in Fig. 2D that at high temperatures, $\Delta E(x)$ follows the illumination beam profile, which is marked by the solid red line (the small increase in the distribution width is due to diffusion). Remarkably, however, as the temperature is lowered below ~6 K, $\Delta E(x)$ becomes constant across the 200-μm wide mesa, while the PL intensity, $I(x)$, continues to follow approximately the illumination beam profile. In fact, we find that the constant ΔE extends a few hundred micrometers further into the leads to the mesa. The lack of correlation between $I(x)$ and $\Delta E(x)$ implies that long-lived particles, which contribute to ΔE but do not emit light, diffuse uniformly throughout the large mesa.

The exchange splitting, ε_{bd}, which is the energy difference between bright and dark excitons, is much smaller than $k_B T$ in GaAs CQW throughout the temperature range studied in this work. Hence, the formation of a large steady-state density of dark excitons implies that a high occupation of the ground state occurs at low temperatures, an indication for a BEC transition. This is corroborated by observation of residual spatial coherence over short lengths in an experiment performed in a trap geometry (11).

The Condensate Loss Mechanisms

The question we wish to focus on in the rest of this article is what determines the density of the condensate. In Fig. 3*A*, we present an Arrhenius plot of the data in Fig. 2*A*, showing $\log(\Delta E_c)$ versus $1/T$. In order to consider the contribution of the dark condensate only, ΔE_c, we subtract $E_{IX}(P,\infty)$, the IX energy at the same power and high temperatures ($T=9$ K), from the measured $E_{IX}(P,T)$, such that $\Delta E_c = E_{IX}(P,T) - E_{IX}(P,\infty)$. This removes the bright exciton contribution, which should be present also at high temperatures. A clear linear behavior is seen for the three voltages with an identical slope. This is a signature of an activated behavior, $\Delta E_c = A\exp(U_0/k_B T)$, and the identical slopes imply that the activation energy is the same at all voltages. (Here the prefactor A is the blueshift at $T=\infty$and U_0 is the height of an effective hard-wall repulsive potential). Repeating this procedure for the data collected at other excitation powers reveals a similar behavior with the same activation energy (inset of Fig. 3*A*). This behavior indicates the existence of a potential barrier, such that when the dark excitons can be thermally excited above it, they are lost and ΔE decreases. Since we do not observe a corresponding drop in the PL intensity as the temperature is reduced, we conclude that the dark excitons are eventually converted into bright ones and are quickly removed from the system by radiative recombination. This suggests that spin-flipping collisions, which convert two dark excitons, $|\pm 2\rangle$, into two bright ones, $|\pm 1\rangle$, through particle exchange, $|+2\rangle + |-2\rangle \rightarrow |+1\rangle + |-1\rangle$, is the loss mechanism determining the condensate density, n_c.

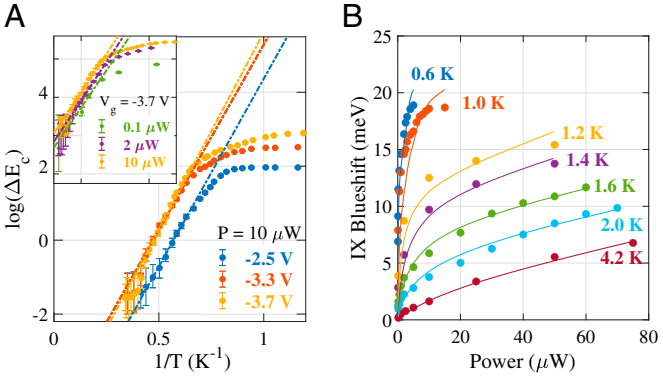

Fig. 3. (*A*) Arrhenius plot showing $\log(\Delta E_c)$ versus 1/T, where $\Delta E_c = E_{IX}(P,T) - E_{IX}(P,\infty)$ is the blueshift due to the condensate only at $P=10$ μW. $E_{IX}(P,T)$ is taken from the data in Fig. 2*A*, and $E_{IX}(P,\infty)$ is the IX energy at the same power and high temperature ($T=9$ K). The dash-dotted lines are linear fits for the data points in the region before the crossing with X_{WW}. Remarkably, the fits give practically same slopes. (*Inset*) The same analysis at $V_g=-3.7$ V for various powers (the *x* and *y* scales are the same as in the main figure). (*B*) Filled circles indicate the measured power dependence of the IX blueshift ΔE at various temperatures at $V_g=-3.7$ V. The maximal $\Delta E=18$ meV is limited by the crossing of the X_{WW} line (Fig. 2*A*). Solid lines indicate the steady-state solutions of the rate-equations model.

We can express the rate of this particle exchange collision process as αn_c^2, where $\alpha = \alpha_0 \exp(-U_0/k_B T)$, and α_0 is the exchange energy density. To extract U_0 from the slope of the linear fits in Fig. 3*A*, we need to express ΔE in terms of n_c. We note that for a condensate $\Delta E \propto n_c^{3/2}$ (20), and hence U_0, is given by three-fourths of that slope. The resulting value for $U_0 \approx 0.5$ meV corresponds to the height of the screened exciton–exciton repulsive potential at $\sim 2a_B$, where a_B is the exciton radius (22). When $k_B T > U_0$, excitons can be excited above this barrier and tunnel into the region $r < 2a_B$, and the proba bility for particle exchange substantially increases.

A confirmation of this picture is provided by examining the power dependence of the blueshift, $\Delta E(P)$, shown in Fig. 3*B*. It is seen that ΔE is sublinear in P at all temperatures. Since ΔE should grow with n_c, it implies that the loss mechanism should be superlinear in n_c. Indeed, if we write the rate equation for n_c as $dn_c/dt \approx P - \alpha n_c^2$, d/dt being the time derivative, we recover the sublinear dependence of ΔE on P. We can use the resulting expression for the steady-state condensate density, $n_c \approx \sqrt{P/\alpha}$, to obtain the exchange energy density, α_0. We find $\alpha_0 \sim 10^{-8}$ m^2 s^{-1}, increasing by a factor of 3 between $V_g=-2.5$ to -3.7 V. This order of magnitude is in very good agreement with the calculation in ref. 21 for the exchange integral using $d=18$ nm, the dipole length in our sample, thereby providing a strong support for this interpretation. We note that the characteristic lifetime for this process is $\sim\sqrt{P\alpha}$ and is a few microseconds for $P=10$ μW.

Rewriting $\alpha = \alpha_0 \exp(-\frac{T_0}{T})$, we can define a characteristic temperature, $T_0 \approx 7$ K, below which this scattering process is exponentially suppressed and the dark-exciton density increases. Hence, the increase in ΔE with reducing temperatures should not be interpreted as the onset of BEC but is rather a manifestation of the exponential inhibition of the two-particle scattering process at $T << T_0$. In other words, the large density of dark excitons, which is observed at low temperatures, implies that a macroscopic occupation of the ground state does occur in this system. However, its diminishing at higher temperatures is not related to exceeding the critical temperature for condensation. This can explain why the temperature below which the blueshift starts to increase is rather constant and does not scale linearly with power as expected for the critical temperature for BEC.

Earlier works that have studied the impact of particle exchange on the condensate (19, 21) focused on the critical density beyond which the condensate becomes gray (e.g., acquires a bright component). At this critical density, the energy correction due to exchange processes between excitons becomes larger than ε_{bd}, and the BEC is a coherent mixture of dark and bright components. While this is true for $T=0$, at a

finite temperature these particle-exchange processes should be active also at densities lower than that critical density and become the dominant loss mechanism of the condensate.

Finally, we wish to emphasize that in most of the power and temperature ranges, the role of nonradiative recombination processes is insignificant in determining the condensate density. Estimate of the nonradiative recombination rate in our sample, $\gamma_{nr} \approx 3 \times 10^3$ s^{-1}, is given in *SI Appendix, Nonradiative Processes*, and it is easy to see that $\alpha n_c^2 \gg \gamma_{nr} n_c$ for $n_c \gtrsim 10^{10}$ cm^{-2} and $T \gtrsim 1$ K. Hence, only at very low powers and temperatures, when spin-flipping processes are suppressed, nonradiative processes become important (21).

The Condensate–Bright Excitons Interaction

To uncover the role of the $J_z = \pm 1$ bright excitons, we preferentially modify their density, n_1, and study the response of the system to this modification. This is achieved by applying a magnetic field parallel to the CQW layers, $\boldsymbol{B}_{||} = \hat{\boldsymbol{x}} B$. Under such a field, the exciton dispersion in the direction normal to it, $\hat{\boldsymbol{y}}$, is shifted such that its minimum is at $k_y = eBd/\hbar$. At $B > 1$ T, this minimum resides outside the radiative zone (e.g., $eBd/\hbar > k_0 = E_{IX}\sqrt{\varepsilon}/\hbar c$), and only a fraction of the excitons can recombine radiatively. Hence, the effective radiative lifetime of the system, τ_r^{eff}, and consequently n_1, are expected to grow with B (23). Indeed, we find a 40-fold increase in the measured lifetime, from 40 ns at $B = 0$ to ≈ 1.6 μs at $B = 4$ T (*SI Appendix*, Fig. S2). To see the effect of this increment in n_1, we examine the behavior at high temperatures, $T > 2K$, where the contribution of the dark excitons to the blueshift is relatively small. Fig. 4*A* shows $\Delta E(B)$ at $T = 2.9$ K for two voltages, $V_g = -2.5$ V and -2.9 V, where we have subtracted the zero-field blueshift due to dark excitons. Indeed, a clear blueshift of the IX energy is seen as the magnetic field is ramped between 0 and 4 T. As expected, the longer zero-field lifetime at $V_g = -2.9$V gives rise to a larger blueshift at 4 T. This magnetic-field–induced ΔE represents a straightforward steady-state exciton accumulation, $n_1 \sim P\tau_r^{eff}$, as opposed to the dark-exciton accumulation at $B = 0$, which is not lifetime related.

A surprising effect is observed at lower temperatures, where n_c becomes significant. We find that $\Delta E(B)$ decreases at low fields, reaches a minimum at $B \sim 2.5$ T and then rises again at higher fields, such that the IX energy at $B = 4$ T is the same for all temperatures (Fig. 4*B*). Dark–bright exciton mixing could be ruled out as the cause of this dip: The effect of such mixing should be observed already at $B_{||} \ll 1$ T; however, as can be seen in Fig. 4*B*, we do not find any significant drop of the IX energy below 1 T (*SI Appendix, Calculation Results* includes an expanded discussion).

This behavior, which is verified to appear in other voltages and powers, can be interpreted as a competition between two opposing trends: An increase of ΔE due to the buildup of the $|\pm 1\rangle$ bright-exciton density, n_1, and a corresponding decrease due to the depletion of the $|\pm 2\rangle$ dark-exciton density, n_c, with increasing magnetic field. We note that the magnitude of the dip in $\Delta E(B)$, which is not present in Faraday configuration measurements, becomes larger with decreasing temperature as the zero-field dark-exciton density, $n_c(B = 0)$, increases. (The data for Faraday configurations are presented in *SI Appendix, Measurements in Magnetic Fields*). We can, therefore, conclude that the depletion of the condensate is proportional to both n_1 and n_c, and can be formally expressed as $\beta n_1 n_c$.

Such a loss term represents interaction between bright and dark excitons. Clearly, particle exchange does not yield a net change in the dark-exciton density in this case. The underlying mechanism can be understood in the following way: It is well known that the dominant spin-flip mechanism of excitons in CQW is the Dyakonov–Perel effect (24). In the single-particle picture of this effect, momentum scattering with impurities changes the direction of the exciton motion in the noncentrosymmetric crystal and gives rise to loss of spin orientation. We suggest that momentum scattering of the dark excitons by the thermal bright excitons, with a rate that can be expressed as $\beta n_1 n_c$, gives rise to a similar effect. It is easy to see that inclusion of this term in the zero-field behavior would yield a saturation of n_c with power at low temperatures, where the αn_c^2 term is suppressed: If we express n_1 as $\approx P/\gamma_r$ and write the rate equation as $dn_c/dt \approx P - \beta n_1 n_c$, we can see that at steady state, $n_c \approx \frac{\gamma_r}{\beta}$. This explains the origin of the saturation of the $\Delta E(P)$ curve at high power, which is observed at $T < 1.5K$ (Fig. 3*B*).

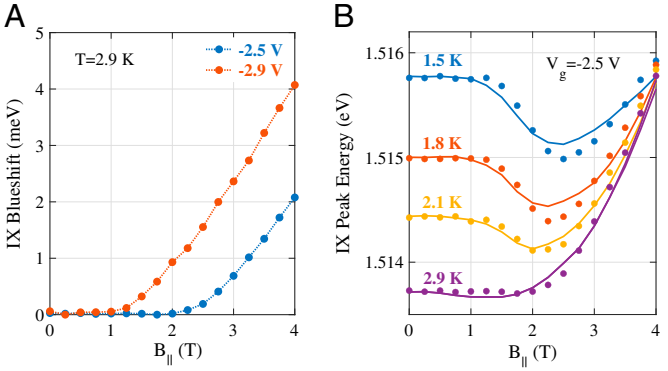

Fig. 4. (*A*) Measured ΔE as a function of in-plane magnetic field at two voltages at P = 10 μw. (*B*) Dots indicate the measured ΔE as a function of $B_{||}$ at several temperatures. Solid lines indicate the calculated behavior using the rate-equations model.

Discussion

The findings we have presented allow us to construct a nonlinear rate-equations model (*SI Appendix, The Rate Equations Model*), which includes the αn_c^2 and $\beta n_1 n_c$ terms for the full system, comprising thermal bright and dark excitons, with steady-state densities n_1 and n_2, respectively, and a condensate of dark excitons, with a steady-state density n_c. The fast decay of the bright excitons through radiative recombination acts as a sink for the system, thereby limiting n_c. The particles exchange among the three reservoirs, n_1, n_2, and n_c, and with the environment, through radiative and nonradiative recombination, γ_r and γ_{nr}, respectively, is schematically depicted in Fig. 5*A*. The thermal bath is pumped at a rate P, and the condensate is formed through stimulated scattering at a rate $W^+ = Rn_2 n_c$. Solving these equations, we obtain the steady-state density of n_1, n_2, and n_c as a function of power and temperature (*SI Appendix, Approximated Solutions* and *Calculation Results*). The total density $n(P, T) = n_1 + n_2 + n_c$ is depicted in Fig. 5*B*, where the increase of n with decreasing temperature at constant power, and the sublinear dependence of n on P, are clearly seen. The solid lines in Figs. 3*B* and 4*B* are best fit to ΔE predicted by this model. It is seen that the fitted lines are in very good agreement with the experimental data. The dark nature of the condensate is, therefore, understood as a result of the unique dynamic properties of the system: the long lifetime of the dark exciton and the suppression of dark–bright spin-flip processes.

In the limit of low power and temperatures, where dark to bright spin-flipping processes are suppressed, the condensate

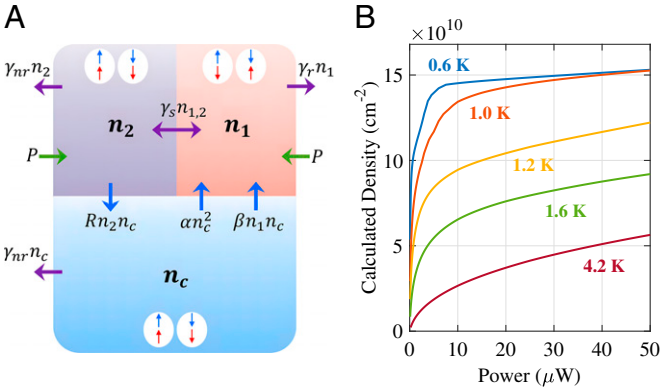

Fig. 5. (*A*) Schematic representation of the particles exchange among the three reservoirs, n_1, n_2, and n_c, and with the environment. The spin orientations of the electron and hole within the excitons are marked by the blue and red arrows, respectively. (*B*) The calculated steady-state total exciton density as a function of excitation power at a few temperatures.

lifetime is determined by nonradiative recombination, and our model converges with that suggested in ref. 21. Indeed, the steep rise of the blueshift with power at $T \leq 1K$ seen in Fig. 5*B* is a manifestation of this effect.

Similar nonlinear loss mechanisms due to interactions among the condensate particles and between them and the thermal bath are known to play an important role in atomic and cavity-polariton condensates (25, 26). In that sense, and in its nonequilibrium nature, the system of dipolar exciton in CQW is very similar to the system of cavity polaritons. We note, however, that the interactions are much stronger in CQW, due to the large electric dipole associated with the IXs, resulting in strong correlation effects (6). Unfortunately, its dark nature makes it difficult to study using spectroscopic tools.

Materials and Methods

The experiments were conducted in a dilution refrigerator with optical windows ($0.05 < T < 6$ K), a variable-temperature, pumped-helium cryostat (1.5 K $< T$) and a variable-temperature, 8-T, split-coil magneto-optic cryostat ($1.5\ K < T$). This allowed us to cover the temperature and magnetic field range of interest of this work: $0.1 < T < 10$ K and $0 < B < 4$ T. For most of the experiments, a Gaussian beam with a 60-μm radius (half width at half maximum) of a continuous wave laser at an energy 1.590 eV illuminated the sample. This energy is well below the barrier height, ensuring carriers are excited in the wells only, and carrier depletion effects are avoided (27). The dark current through the sample at the relevant voltage range was ∼100 pA, and the photocurrent at the highest excitation power, 100 μW, was below 1 nA. The PL from the sample was guided to a U-1000 Jobin-Yvon Raman spectrometer to collect the spectra and analyze them, and was imaged on a cooled Electron-Multiplying Charge-Coupled Device camera (Andor iXon Ultra) with a spatial resolution of 3 μm. Spatially resolved spectroscopic measurements were performed using a pinhole of diameter 20 μm placed at the focal plane of the collection objective. This allowed selective collection of emitted light from various distinct areas of the mesa for imaging and spectroscopic analyses.

We carried out time-resolved measurements to determine the lifetime of IXs using a correlated photon-counting system. To pulse the continuous-wave laser, we used an acousto-optic modulator with a rise time of 17 ns, and an avalanche photodiode (APD) was used to detect the photon events. The pulse duration was 1 μs in a 10-μs duty cycle. The pulses to the acousto-optic modulator and the measurement time windows at the APD were synchronized by a fast arbitrary waveform generator (Tabor AWG WX1284) and a National Instruments Data Acquisition card was used for counting the APD output.

Data Availability. The data used in the article and the supporting information are available on the Open Science Framework (OSF) (https://osf.io/fnhrg/) (28). Further supporting data and codes used for analyses and modeling are available from the corresponding author upon reasonable request.

ACKNOWLEDGMENTS. This work is supported by the Israeli Science Foundation, Grant 2139/20, and by the Minerva foundation.

1. L. V. Keldysh, A. N. Kozlov, Collective properties of excitons in semiconductors. *Sov. Phys. JETP* **27**, 521 (1968).
2. S. A. Moskalenko, D. W. Snoke, *Bose-Einstein Condensation of Excitons and Biexcitons and Coherent Nonlinear Optics with Excitons* (Cambridge University Press, 2000).
3. Yu. E. Lozovik, V. I. Yudson, Feasibility of superfluidity of paired spatially separated electrons and holes; a new superconductivity mechanism. *JETP Lett.* **22**, 274 (1975).
4. D. W. Snoke, Coherence and optical emission from bilayer exciton condensates. *Adv. Condens. Matter Phys.* 938609 (2011).
5. M. Combescot, R. Combescot, F. Dubin, Bose-Einstein condensation and indirect excitons: A review. *Rep. Prog. Phys.* **80**, 066501 (2017).
6. Yu. E. Lozovik, I. L. Kurbakov, G. E. Astrakharchik, J. Boronat, M. Willander, Strong correlation effects in 2D Bose-Einstein condensed dipolar excitons. *Solid State Commun.* **144**, 399–404 (2007).
7. A. V. Gorbunov, V. B. Timofeev, Large-scale coherence of the Bose condensate of spatially indirect excitons. *JETP Lett.* **84**, 329–334 (2006).
8. A. A. High *et al.*, Spontaneous coherence in a cold exciton gas. *Nature* **483**, 584–588 (2012).
9. Y. Shilo *et al.*, Particle correlations and evidence for dark state condensation in a cold dipolar exciton fluid. *Nat. Commun.* **4**, 2335 (2013).
10. M. Stern, V. Umansky, I. Bar-Joseph, Exciton liquid in coupled quantum wells. *Science* **343**, 55–57 (2014).
11. M. Alloing *et al.*, Evidence for a Bose-Einstein condensate of excitons. *Europhys. Lett.* **107**, 10012 (2014).
12. K. Cohen, Y. Shilo, K. West, L. Pfeiffer, R. Rapaport, Dark high density dipolar liquid of excitons. *Nano Lett.* **16**, 3726–3731 (2016).
13. M. Beian *et al.*, Spectroscopic signatures for the dark Bose-Einstein condensation of spatially indirect excitons. *Europhys. Lett.* **119**, 37004 (2017).
14. R. Anankine *et al.*, Quantized vortices and four-component superfluidity of semiconductor excitons. *Phys. Rev. Lett.* **118**, 127402 (2017).
15. S. Misra, M. Stern, A. Joshua, V. Umansky, I. Bar-Joseph, Experimental study of the exciton gas-liquid transition in coupled quantum wells. *Phys. Rev. Lett.* **120**, 047402 (2018).
16. S. Dang *et al.*, Defect proliferation at the quasicondensate crossover of two-dimensional dipolar excitons trapped in coupled GaAs quantum wells. *Phys. Rev. Lett.* **122**, 117402 (2019).
17. Z. Wang *et al.*, Evidence of high-temperature exciton condensation in two-dimensional atomic double layers. *Nature* **574**, 76–80 (2019).
18. M. Combescot, O. Betbeder-Matibet, R. Combescot, Bose-Einstein condensation in semiconductors: The key role of dark excitons. *Phys. Rev. Lett.* **99**, 176403 (2007).
19. R. Combescot, M. Combescot, "Gray" BCS condensate of excitons and internal Josephson effect. *Phys. Rev. Lett.* **109**, 026401 (2012).
20. B. Laikhtman, R. Rapaport, Exciton correlations in coupled quantum wells and their luminescence blue shift. *Phys. Rev. B Condens. Matter Mater. Phys.* **80**, 195313 (2009).
21. Y. Mazuz-Harpaz *et al.*, Dynamical formation of a strongly correlated dark condensate of dipolar excitons. *Proc. Natl. Acad. Sci. U.S.A.* **116**, 18328–18333 (2019).
22. R. Zimmermann, C. Schindler, Exciton-exciton interaction in coupled quantum wells. *Solid State Commun.* **144**, 395–398 (2007).
23. L. V. Butov, A. V. Mintsev, Yu. E. Lozovik, K. L. Campman, A. C. Gossard, From spatially indirect excitons to momentum-space indirect excitons by an in-plane magnetic field. *Phys. Rev. B Condens. Matter Mater. Phys.* **62**, 1548 (2000).
24. M. I. Dyakonov, Ed., *Spin Physics in Semiconductors.* Springer Series on Solid State Physics 157. (Springer, 2017).
25. D. Jaksch, C. W. Gardiner, K. M. Gheri, P. Zoller, Quantum kinetic theory. IV. Intensity and amplitude fluctuations of a Bose-Einstein condensate at finite temperature including trap loss. *Phys. Rev. A* **58**, 1450 (1998).
26. I. Carusotto, C. Ciuti, Quantum fluids of light. *Rev. Mod. Phys.* **85**, 299 (2013).
27. R. Rapaport *et al.*, Charge separation of dense two-dimensional electron-hole gases: Mechanism for exciton ring pattern formation. *Phys. Rev. Lett.* **92**, 117405 (2004).
28. S. Misra, Data for "The role of spin-flip collisions in a dark exciton condensate." OSF. https://osf.io/fnhrg/. Deposited 19 July 2022.